

# Separating a particle's mass from its momentum

Mordecai Waegell<sup>a,\*</sup>, Jeff Tollaksen<sup>a,b</sup>, and Yakir Aharonov<sup>a,b,c,d</sup>

<sup>a</sup>Institute for Quantum Studies, Chapman University, 1 University Dr., Orange, CA 92866, USA

<sup>b</sup>Schmid College of Science and Technology, Chapman University, 450 N Center St., Orange, CA 92866, USA

<sup>c</sup>Iyar, The Israeli Institute for Advanced Research, POB 651 Zichron Ya'akov 3095303, Israel

<sup>d</sup>School of Physics and Astronomy, Tel Aviv University, Tel Aviv, Israel

\*Corresponding Author, email: waegell@chapman.edu

January 22, 2024

## Abstract

The Quantum Cheshire Cat experiment showed that when weak measurements are performed on pre- and post-selected system, the counterintuitive result has been obtained that a neutron is measured to be in one place without its spin, and its spin is measured to be in another place without the neutron. A generalization of this effect is presented with a massive particle whose mass is measured to be in one place with no momentum, while the momentum is measured to be in another place without the mass. The new result applies to any massive particle, independent of its spin or charge. A *gedanken* experiment which illustrates this effect is presented using a nested pair of Mach-Zehnder interferometers, but with some of the mirrors and beam splitters moving relative to the laboratory frame. The analysis of this experiment using the counterparticle ontology of Aharonov et al. is also given.

## 1 Introduction

The time-symmetric quantum formalism of Aharonov, Bergmann, and Lebowitz [1] offers a unique perspective on situations where measurements are conditioned on a particular post-selection of the measured system, and if the coupling of the

measurement device and system is so weak that it reveals very little information per run, the conditioned ensemble average, called a weak value [2], [3], can exhibit counterintuitive behavior. Thinking about experiments in terms of time-symmetric boundary conditions, i.e, a pre-selected state, a post-selected state, and the weak values which are defined by this pair during the intermediate time, has led to a number of interesting results that would have been much less obvious in the standard treatment [4]–[11]. To apply this reasoning, one must think of both the pre-selected (prepared) and post-selected (outcome) state as existing ‘first,’ and the choice of intermediate measurement settings as existing ‘second,’ which is quite contrary to our usual intuition that ‘first’ and ‘second’ should match their temporal order.

Our goal in this article is to present a variation of the Quantum Cheshire Cat experiment [12], where the mass and spin of a single neutron were separated in the sense that post-selected weak measurements of the position of the neutron find it in location 1 and not location 2, while weak measurements of the neutron spin find spin in location 2 and not in location 1.

Here we instead consider a massive particle whose position can be detected via its gravitational field, and whose momentum can be detected via an impulsive coupling, and show that post-selected grav-

itational weak measurements of the position of the mass find it in location 1 and not location 2, while impulsive weak measurements of the momentum find nonzero momentum in location 2 and zero in location 1. In this sense, we show that the momentum of the particle has been separated from its mass. Most of the kinetic energy is separated in the same way, although an arbitrarily small amount remains with the mass. This effect is related to interaction-free energy transfer [13], where the weak value of the projector onto one arm of the interferometer is zero, while the weak value of the energy on that arm is nonzero.

Our results apply to any massive particle, and thus generalize the original Quantum Cheshire Cat Effect. In the *gedanken* experiment we introduce, the position of the mass is detected via the gravitational force, but the mirrors, beam splitters, and impulsive detectors must interact with the particle through other forces, regardless of which forces they are.

## 2 The Pre-Selected and Post-Selected States

We begin by constructing the desired pre-and post-selected states to show the effect, and then we provide some details of a *gedanken* experiment to produce these states. We begin by constructing three different normalized Gaussian states,  $f_{\pm}(x)$  and  $g(x)$ . The functions  $f_{\pm}(x)$  are centered at the origin with average momenta given by  $k_0 \pm k_1$ , while the function  $g(x)$  has zero average momentum and it is centered at  $x_0$ .

$$f_{\pm}(x) = \left(\frac{2\Delta k_f^2}{\pi}\right)^{1/4} e^{i(k_0 \pm k_1)x} e^{-x^2/4\Delta k_f^2} \quad (1)$$

$$\tilde{f}_{\pm}(k) = \left(\frac{1}{2\pi\Delta k_f^2}\right)^{1/4} e^{-(k-(k_0 \pm k_1))^2/4\Delta k_f^2} \quad (2)$$

$$g(x) = \left(\frac{2\Delta k_g^2}{\pi}\right)^{1/4} e^{-(x-x_0)^2/4\Delta k_g^2} \quad (3)$$

$$\tilde{g}(k) = \left(\frac{1}{2\pi\Delta k_g^2}\right)^{1/4} e^{ikx_0} e^{-k^2/4\Delta k_g^2} \quad (4)$$

From  $f_{\pm}$  we construct two new (unnormalized) states  $h_{\pm}$  as,

$$h_+ \equiv f_+ + f_-, \quad h_- \equiv f_+ - f_-. \quad (5)$$

Note that  $f_+$  and  $f_-$  are not orthogonal, but  $h_+$  and  $h_-$  are,

$$\langle f_+ | f_- \rangle = e^{-k_1^2/2\Delta k_f^2}, \quad \langle h_+ | h_- \rangle = 0. \quad (6)$$

From these and  $g$  we construct our (unnormalized) pre- and post-selected states,  $\psi$  and  $\phi$ , respectively.

$$\psi = g + h_+, \quad \phi = g + h_-. \quad (7)$$

## 3 Weak Values

The weak value of any operator  $\hat{A}$  on this system is defined as

$$\hat{A}_w \equiv \frac{\langle \phi | \hat{A} | \psi \rangle}{\langle \phi | \psi \rangle}. \quad (8)$$

We set  $x_0 \gg \Delta x_g = 1/(2\Delta k_g)$  and  $x_0 \gg \Delta x_f = 1/(2\Delta k_f)$  so that  $\langle f_{\pm} | g \rangle \approx 0$  and thus  $\langle h_{\pm} | g \rangle \approx 0$ . Then we have

$$\langle \phi | \psi \rangle \approx \langle g | g \rangle = 1, \quad (9)$$

so we can neglect the denominator in Eq. 8 when finding weak values.

We now define projectors onto two separate regions of the  $x$ -axis;  $\hat{\Pi}_h$  is the region where  $h_{\pm}(x)$  have support and  $g(x)$  has almost none, and vice versa for  $\hat{\Pi}_g$ . As an approximation, we will define these projectors so that they perfectly isolate the two functions. Applying these operators to  $\psi(x)$  we have,

$$\begin{aligned} \hat{\Pi}_h | \psi \rangle &= | h_+ \rangle, & \hat{\Pi}_g | \psi \rangle &= | g \rangle, \\ \langle \phi | \hat{\Pi}_h^\dagger &= \langle h_- |, & \langle \phi | \hat{\Pi}_g^\dagger &= \langle g |. \end{aligned} \quad (10)$$

We are now in a position to consider the weak values of the projectors onto these regions, along with the localized energy and momentum in each region.

For the projectors alone we have,

$$\begin{aligned} (\hat{\Pi}_h^\dagger \hat{\Pi}_h)_w &= \langle \phi | \hat{\Pi}_h^\dagger \hat{\Pi}_h | \psi \rangle = 0, \\ (\hat{\Pi}_g^\dagger \hat{\Pi}_g)_w &= \langle \phi | \hat{\Pi}_g^\dagger \hat{\Pi}_g | \psi \rangle = 1, \end{aligned} \quad (11)$$

so the particle seems be located entirely in the region spanned by  $\hat{\Pi}_g$ .

For the localized momentum we have,

$$\begin{aligned} (\hat{\Pi}_h^\dagger p \hat{\Pi}_h)_w &= \langle \phi | \hat{\Pi}_h^\dagger p \hat{\Pi}_h | \psi \rangle = 2p_1 = 2\hbar k_1, \\ (\hat{\Pi}_g^\dagger p \hat{\Pi}_g)_w &= \langle \phi | \hat{\Pi}_g^\dagger p \hat{\Pi}_g | \psi \rangle = 0, \end{aligned} \quad (12)$$

so the localized momentum at the apparent location of the particle ( $\hat{\Pi}_g$ ) is zero, while the localized momentum in the region where the particle is not located ( $\hat{\Pi}_h$ ) is  $2p_1$ .

For the localized energy we have,

$$\begin{aligned} \left( \frac{\hat{\Pi}_h^\dagger p^2 \hat{\Pi}_h}{2m} \right)_w &= \frac{1}{2m} \langle \phi | \hat{\Pi}_h^\dagger p^2 \hat{\Pi}_h | \psi \rangle = \frac{2p_0 p_1}{m} = \frac{2\hbar^2 k_0 k_1}{m}, \\ \left( \frac{\hat{\Pi}_g^\dagger p^2 \hat{\Pi}_g}{2m} \right)_w &= \frac{1}{2m} \langle \phi | \hat{\Pi}_g^\dagger p^2 \hat{\Pi}_g | \psi \rangle = \frac{\Delta p_g^2}{2m} = \frac{\hbar^2 \Delta k_g^2}{2m}. \end{aligned} \quad (13)$$

Now, in the limit that  $\Delta k_g = (1/2\Delta x_g)$  is very close to zero, the localized energy at the apparent location of the particle ( $\hat{\Pi}_g$ ) is also nearly zero, while the localized energy in the region where the particle is not located ( $\hat{\Pi}_h$ ) may be much larger.

So for these pre- and post-selected states, with parameters chosen so that  $0 \ll \Delta x_g \ll x_0$  and  $\Delta x_f \ll x_0$ , we have our generalization of the Quantum Cheshire Cat effect: The mass is located in one place without momentum, and the momentum is located elsewhere without mass. Note that neither  $k_0$  nor  $k_1$  needed to be constrained to see this effect, so there is no bound on the energy or momentum of the particle.

## 4 Gedanken Experiment

To measure the momentum and energy, it should be sufficient to perform a local impulsive coupling with a broadly spread pointer in region  $h$  and another in region  $g$ . The pointers will weakly measure that there is momentum in region  $h$  and none in region  $g$ . It does not matter what force mediates the impulsive couplings, mirrors, and beam splitters. Another pair of pointers will couple via the gravitational interaction, and these will find mass located in region  $g$  but none in region  $h$ .

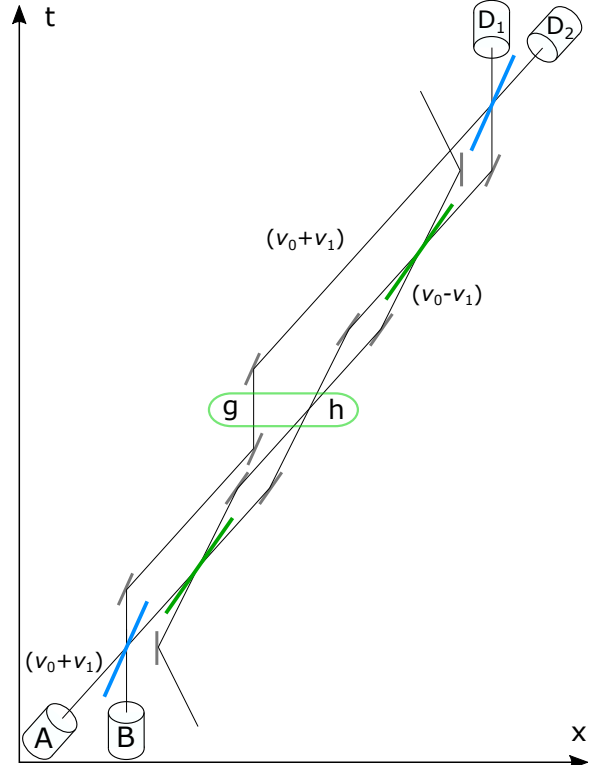


Figure 1: The one-dimensional experimental setup for the energy-momentum Quantum Cheshire Cat effect, with all forward and backward paths shown. The tilts of the mirrors (gray), beam splitters (blue and green), and trajectories show their velocities ( $\frac{1}{2}(v_0 + v_1)$  for blue, and  $v_0$  for green), while the sources and detectors are at the shown events.

To accomplish this, we consider a setup which has some resemblance to the nested interferometers used by Vaidman [5], but we will use a massive particle moving at nonrelativistic speeds, and some of the mirrors and beam splitters that are used to redirect the particle will also be moving. The experimental setup is shown in Fig. 1 as a space-time diagram depicting motion in one dimension. Because this is one-dimensional, the tilt of the mirrors and beam splitters represents their velocities (it shows the direction of their world-lines), and likewise for the tilt of the particle trajectories.

To prepare the desired pre-selected state, we begin by sending a Gaussian wave packet  $f_+$  ( $v = \hbar k/m$  and  $v_+ \equiv v_0 + v_1$ ) into our apparatus, and then passing it through a beam splitter moving with velocity  $\frac{1}{2}v_+$ , such that one path comes to rest at  $x_0$  ( $g$ ) and the other propagates with velocity  $v_+$  ( $f_+$ , and we have  $\Delta k_f = \Delta k_g$ , since they split off from the same packet). To see this, consider the situation in the rest frame of the beam splitter, where the velocity of the incoming particle is  $v'_+ = v_+ - \frac{1}{2}v_+ = \frac{1}{2}v_+$ . The resting beam splitter then naturally results in a reflected path with velocity  $-\frac{1}{2}v_+$ , and a transmitted path with velocity  $\frac{1}{2}v_+$ . Returning to the original frame where the beam splitter has velocity  $\frac{1}{2}v_+$ , we see that the reflected path has velocity  $v_r = -\frac{1}{2}v_+ + \frac{1}{2}v_+ = 0$  and the transmitted path has the original velocity  $v_t = \frac{1}{2}v_+ + \frac{1}{2}v_+ = v_+$ . Also, reflection from mirrors moving at  $\frac{1}{2}v_+$  swaps between  $v_+$  and 0.

Similarly, when a particle with velocity  $v_+$  is incident on another beam splitter with velocity  $v_0$ , the reflected path has velocity  $v_r = v_- \equiv (v_0 - v_1)$ , and  $v_+$  for the transmitted path. Also, reflection from mirrors moving at  $v_0$  swaps between  $v_+$  and  $v_-$ .

We now have all of the components of our apparatus, and we know how they will interact with incoming particles at velocities  $v_+$  and  $v_-$ , which is everything we need for the experiment. Consider the pre-selection where the particle is sent in along path  $A$ . Fig. 2 shows trajectories for all parts of the superposition state that propagate through the apparatus from  $A$ . We can see that the upper path leads to the two detectors, while the lower path ultimately escapes the apparatus undetected. For our post-selection, we consider the case that detector  $D_2$  fires, which only appears to be possible if the particle traversed the upper path. Fig. 3 shows trajectories for all parts of the superposition state obtained by back-propagating through the apparatus from  $D_2$ . We can see that the upper path leads back to the input ports, but the lower path leads out of an unused input port of the apparatus.

To choose the reflectivity of the our first beam splitter, we need to consider the normalized pre-

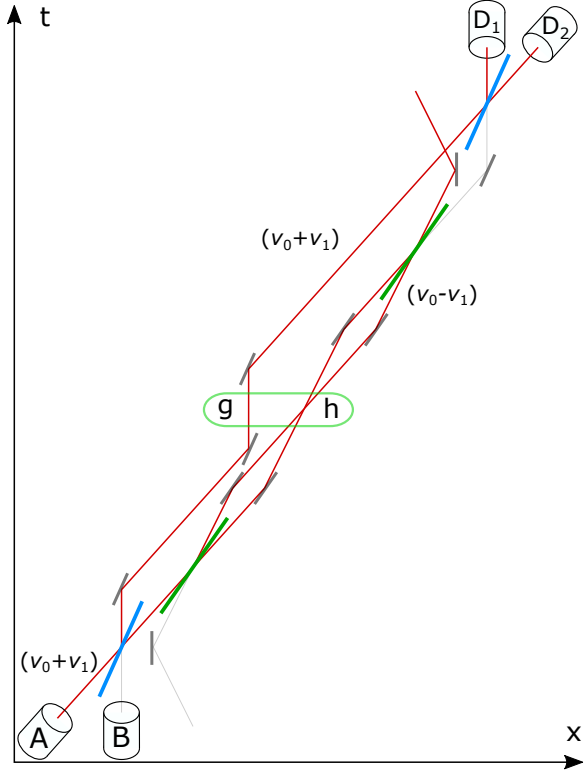


Figure 2: The experimental setup with the particle pre-selected to enter from source A with velocity  $v_+ = v_0 + v_1$ . All subsequent places where the pulse has nonzero support are shown in red.

selection

$$\psi(x) = \frac{g(x) + f_+(x) + f_-(x)}{\sqrt{3 + 2e^{-k_1^2/2\Delta k_f^2}}}. \quad (14)$$

The first beam splitter (speed  $\frac{1}{2}v_+$ ) is tuned so that

$$\frac{1}{3 + 2e^{-k_1^2/2\Delta k_f^2}} \quad (15)$$

of the intensity of the beam is reflected ( $v_r = 0$ ), and

$$\frac{2 + 2e^{-k_1^2/2\Delta k_f^2}}{3 + 2e^{-k_1^2/2\Delta k_f^2}} \quad (16)$$

is transmitted ( $v_t = v_+$ ). The second beam splitter (speed  $v_0$ ) then transforms the  $v_+$  term into an

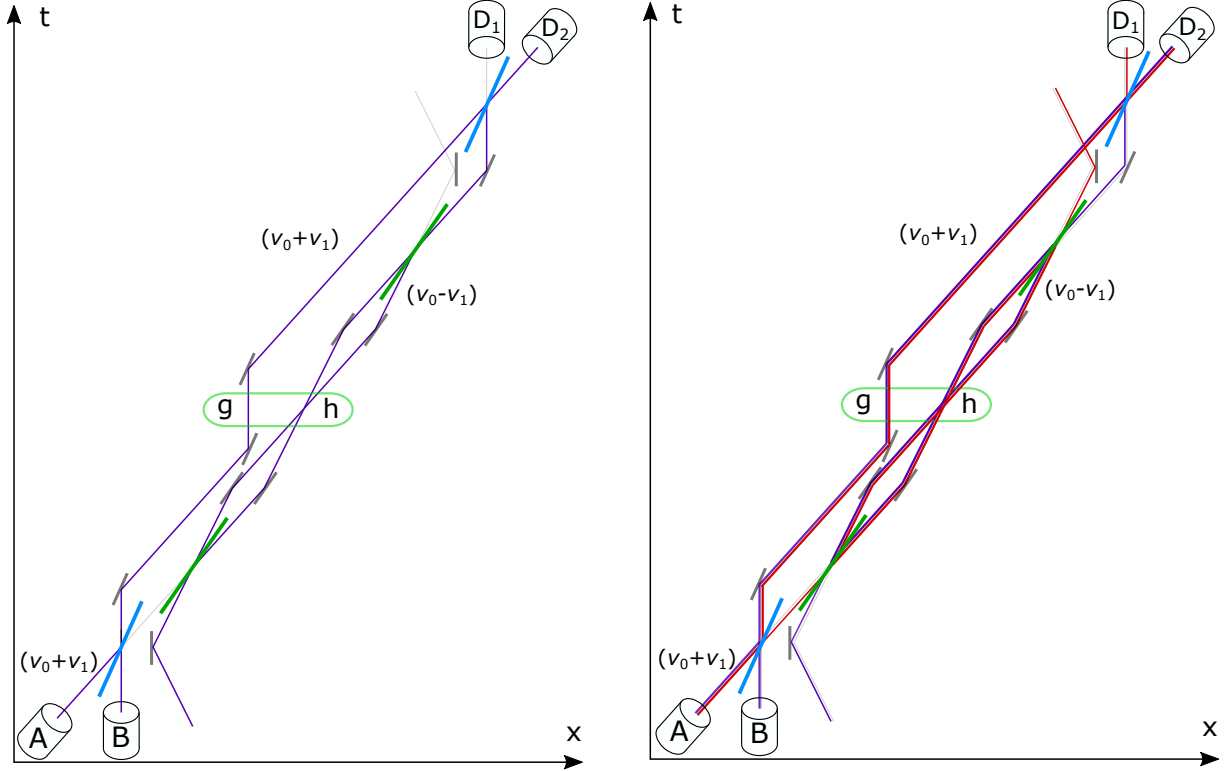


Figure 3: The experimental setup with the particle post-selected to exit at detector  $D_2$  with velocity  $v_+ = v_0 + v_1$ . All places where the back-propagated pulse has nonzero support are shown in dark purple.

equal superposition of  $v_+$  and  $v_-$  (with no phase difference), which gives us  $\psi$  once the packets arrive in the target region.

To choose the reflectivity of our final beam splitter, we consider the normalized post-selection

$$\phi(x) = \frac{g(x) + f_+(x) - f_-(x)}{\sqrt{3 - 2e^{-k_1^2/2\Delta k_f^2}}}. \quad (17)$$

The final beam splitter (speed  $\frac{1}{2}v_+$ ) is tuned so that fraction

$$\frac{1}{3 - 2e^{-k_1^2/2\Delta k_f^2}} \quad (18)$$

of a back-propagated beam from  $D_2$  is transmitted

Figure 4: The experimental setup with all trajectories forward from the pre-selection in red, and all trajectories backward from the post-selection in dark purple. Nonzero weak values are only found in the regions where the two overlaps, which are shown with thicker lines.

back toward region  $g$  (speed  $v_+$ ), and fraction

$$\frac{2 - 2e^{-k_1^2/2\Delta k_f^2}}{3 - 2e^{-k_1^2/2\Delta k_f^2}} \quad (19)$$

is reflected toward region  $h$  (speed 0). The third beam splitter (speed  $v_0$ ) then transforms the  $v_+$  term into an equal superposition of  $v_+$  and  $v_-$  with a  $\pi$  phase difference between the terms, which gives us  $\phi$  once the packets are back-propagated to the target region.

## 5 Analysis

In this experiment, we find that the weak value of the particle's momentum in region  $h$  is  $2p_1$ , while the weak value of its position places it squarely in the region  $g$ . Furthermore, if the particle must follow a physically consistent trajectory from the pre-selection to the post-selection, it could only have gone by the path through region  $g$ , and indeed we detect no mass in region  $h$ . However, if we consider the joint observables of the momentum in region  $g$  and the momentum in region  $h$ , we find that all of the  $2p_1$  momentum is located in region  $h$  and none in region  $g$  - so the particle is in one place, and its momentum is in another.

The weak value of the particle's kinetic energy is  $\frac{1}{2m}(4p_0p_1 + \Delta p_f^2)$ , and if we look at the joint observables of the energy in regions  $g$  and  $h$ , we find that the  $\frac{\Delta p_f^2}{2m}$  is in region  $g$  and the  $\frac{2p_0p_1}{m}$  is located in region  $h$ . Since we can vary  $p_0$ ,  $p_1$ , and  $\Delta p_f$  more or less freely, and the regions  $g$  and  $h$  can be made arbitrarily far apart, it is easy to arrange it so that the vast majority of the particle's kinetic energy is located in  $h$  (along with its momentum), even though the particle is located in  $g$ .

As in Vaidman's original nested interferometer setup [5], [14], there are regions where the particle leaves no weak trace on the way in or out, but does leave weak traces between those regions, where it should not have been able to go. If we consider the pre- and post-selection, and the mirrors and beam splitter of the outer interferometer to be 'first', we can then make a choice about whether to add the inner interferometer 'second.' If all mirrors and beam splitters of the inner interferometer are absent, only the pre-and post-selected paths through region  $g$  overlap, so all weak values measured outside region  $g$  would be zero all the way through, so it looks as if there is nothing there. What is remarkable is that if our moving inner interferometer is present, we have added some measurable energy and momentum to this nothing.

To see how this works, it is also helpful to consider the weak traces left on the arms of the inner interferometer when the packets are well-separated (outside the region  $h$ ). The packets  $f_+$  and  $f_-$  are only truly

separate and orthogonal in the limit  $k_1^2/\Delta k_f^2 \rightarrow \infty$ , so we consider this case first. In this limit, we can define projectors onto  $f_+$  and  $f_-$ ,

$$\begin{aligned} \hat{\Pi}_{f_+}|\psi\rangle &= |f_+\rangle, & \hat{\Pi}_{f_-}|\psi\rangle &= |f_-\rangle, \\ \langle\phi|\hat{\Pi}_{f_+}^\dagger &= \langle f_+|, & \langle\phi|\hat{\Pi}_{f_-}^\dagger &= -\langle f_-|, \end{aligned} \quad (20)$$

and evaluate their weak values and the corresponding energy and momentum weak values,

$$\begin{aligned} (\hat{\Pi}_{f_\pm}^\dagger \hat{\Pi}_{f_\pm})_w &= \pm 1, & (\hat{\Pi}_{f_\pm}^\dagger p \hat{\Pi}_{f_\pm})_w &= \pm(p_0 \pm p_1), \\ \frac{1}{2m}(\hat{\Pi}_{f_\pm}^\dagger p^2 \hat{\Pi}_{f_\pm})_w &= \pm \frac{1}{2m}((p_0 \pm p_1)^2 + \Delta p_f^2). \end{aligned} \quad (21)$$

Thus, the projectors onto the separate functions have equal and opposite weak values, just as in Vaidman's case. At the crossing point ( $h$ ) the positive and negative projector weak values cancel out, while the energy and momentum remain finite.

When the packets are well-separated, we have effectively three locations to find the particle,  $g$ ,  $f_+$ , and  $f_-$ , and the projector weak values are  $+1$ ,  $+1$ , and  $-1$ , respectively, so we have a case of the 3-box paradox [11].

The presence of negative projector weak values also establishes that quantum contextuality [15]–[18] plays some role in this effect, which is unsurprising given its known relation to other counterintuitive results obtained using time-symmetric quantum mechanics [8], [10].

### 5.1 The Counterparticle Picture

In the retrocausal weak-value-based picture of Aharonov, et al. [9], [11], this is explained by the presence of an extra positive-negative pair of (counter)particles that are created at source A (see Fig. 4) during the pre-selection, propagate together into the inner interferometer (leaving no trace), then take separate paths through the inner interferometer (crossing in region  $h$ ), and then propagate together out of the inner interferometer (again leaving no trace) and are annihilated at  $D_2$  during the post-selection.

Inside the inner interferometer, the negative particle carries negative kinetic energy,  $-\frac{1}{2m}((p_0 - p_1)^2 + \Delta p_f^2)$  and negative momentum (opposite the direction of propagation),  $-(p_0 - p_1)$  and the positive particle carries positive kinetic energy,  $\frac{1}{2m}((p_0 + p_1)^2 + \Delta p_f^2)$  and momentum,  $(p_0 + p_1)$ , but their magnitudes are not equal, resulting in net positive momentum and energy. In the limit  $k_1^2/\Delta k_f^2 \rightarrow \infty$ , these are the weak values for packets  $f_+$  and  $f_-$ , and they sum to the values found for region  $h$  (even outside the limit). As such, we will argue that even outside the limit we still have this positive-negative pair of counterparticles propagating through the apparatus, in addition to some other complicated effects due to the cross-terms that we leave for future analysis.

Thus both the weak values measured when the packets are well-separated and the weak values measured when they fully overlap are explained by the wave packets of a positive-negative pair of counterparticles passing through the apparatus.

A second argument for the presence of the positive-negative pair can be given by modifying the experiment to include entanglement with the internal spin of the particle. If we choose the pre-selection and post-selection to be

$$|\psi\rangle = g|\uparrow\rangle + f_+|\rightarrow\rangle + f_-|\leftarrow\rangle, \quad (22)$$

and

$$|\psi\rangle = g|\uparrow\rangle + f_+|\rightarrow\rangle - f_-|\leftarrow\rangle, \quad (23)$$

then the orthogonal spin states allow us to separate  $f_+$  and  $f_-$ , even outside the limit where  $k_1^2/\Delta k_f^2 \rightarrow \infty$ , we get all of the same weak values of Eq. 21, and there are no cross terms.

A positive-negative pair of particles also explains the weak values in Vaidman's original nested interferometer [5], [9], [11], and a pair with net negative energy and momentum explains the weak values in interaction free energy transfer [13], [19].

## 6 Conclusions

We have presented a variant of the Quantum Cheshire Cat effect where weak measurements of a pre- and post-selected system show that the mass of a

particle is entirely separated from its momentum, and mostly separated from its energy. We have also given a *gedanken* experiment that realizes the necessary pre- and post-selection using nested interferometers which are in motion in the laboratory frame. This is yet another counterintuitive prediction of quantum theory which is relatively straightforward in the two-vector quantum formalism of ABL, but would have been difficult to conceive in the usual one-vector quantum formalism. This result adds to a growing list of remarkable quantum phenomena discovered in this way.

Finally, we have shown how the retrocausal counterparticle ontology of Aharonov et al. provides an intuitive explanation of the relevant weak values in this experiment, using particles that move on definite trajectories through the experiment.

## References

- [1] Y. Aharonov, P. G. Bergmann, and J. L. Lebowitz, "Time symmetry in the quantum process of measurement," *Phys. Rev.*, vol. 134, no. 6B, B1410, 1964.
- [2] Y. Aharonov, D. Z. Albert, and L. Vaidman, "How the result of a measurement of a component of the spin of a spin-1/2 particle can turn out to be 100," *Phys. Rev. Lett.*, vol. 60, no. 14, p. 1351, 1988.
- [3] J. Dressel, "Weak values as interference phenomena," *Physical Review A*, vol. 91, no. 3, p. 032116, 2015.
- [4] Y. Aharonov, S. Popescu, D. Rohrlich, and P. Skrzypczyk, "Quantum cheshire cats," *New Journal of Physics*, vol. 15, no. 11, p. 113015, 2013.
- [5] L. Vaidman, "Past of a quantum particle," *Physical Review A*, vol. 87, no. 5, p. 052104, 2013.
- [6] Y. Aharonov, E. Cohen, and S. Popescu, "A current of the cheshire cat's smile: Dynamical analysis of weak values," *arXiv preprint arXiv:1510.03087*, 2015.

[7] Y. Aharonov, F. Colombo, S. Popescu, I. Sabadini, D. C. Struppa, and J. Tollaksen, “Quantum violation of the pigeonhole principle and the nature of quantum correlations,” *PNAS*, vol. 113, no. 3, pp. 532–535, 2016.

[8] M. Waegell, T. Denkmayr, H. Geppert, *et al.*, “Confined contextuality in neutron interferometry: Observing the quantum pigeonhole effect,” *Physical Review A*, vol. 96, no. 5, p. 052131, 2017.

[9] Y. Aharonov, E. Cohen, M. Waegell, and A. Elitzur, “The weak reality that makes quantum phenomena more natural: Novel insights and experiments,” *Entropy*, vol. 20, no. 11, p. 854, 2018.

[10] M. Waegell and J. Tollaksen, “Contextuality, pigeonholes, cheshire cats, mean kings, and weak values,” *Quantum Studies: Mathematics and Foundations*, vol. 5, no. 2, pp. 325–349, 2018.

[11] M. Waegell, E. Cohen, A. Elitzur, J. Tollaksen, and Y. Aharonov, “Quantum reality with negative-mass particles,” *Proceedings of the National Academy of Sciences*, vol. 120, no. 32, e2018437120, 2023.

[12] T. Denkmayr, H. Geppert, S. Sponar, *et al.*, “Observation of a quantum cheshire cat in a matter-wave interferometer experiment,” *Nature communications*, vol. 5, p. 4492, 2014.

[13] C. Elouard, M. Waegell, B. Huard, and A. N. Jordan, “An interaction-free quantum measurement-driven engine,” *Foundations of Physics*, vol. 50, pp. 1294–1314, 2020.

[14] A. Ben-Israel, L. Knips, J. Dziewior, *et al.*, “An improved experiment to determine the ‘past of a particle’ in the nested mach–zehnder interferometer,” *Chinese Physics Letters*, vol. 34, no. 2, p. 020301, 2017.

[15] S. Kochen and E. Specker, “The problem of hidden variables in quantum mechanics,” *J. of Math. and Mech.*, vol. 17, pp. 59–87, 1967.

[16] R. W. Spekkens, “Contextuality for preparations, transformations, and unsharp measurements,” *Phys. Rev. A*, vol. 71, no. 5, p. 052108, 2005.

[17] M. F. Pusey, “Anomalous weak values are proofs of contextuality,” *Phys. Rev. Lett.*, vol. 113, no. 20, p. 200401, 2014.

[18] R. Kunjwal, M. Lostaglio, and M. F. Pusey, “Anomalous weak values and contextuality: Robustness, tightness, and imaginary parts,” *arXiv preprint arXiv:1812.06940*, 2018.

[19] M. Waegell, C. Elouard, and A. N. Jordan, “Energy-based weak measurement,” *Quantum Studies: Mathematics and Foundations*, pp. 1–6, 2020.